

# Formation and structure of vacancy defects in silicon: Combined Metropolis Monte Carlo, tight-binding molecular dynamics, and density functional theory calculations

Sangheon Lee, Robert J. Bondi, and Gyeong S. Hwang\*

*Department of Chemical Engineering, University of Texas, Austin, Texas 78712, USA*

(Received 23 July 2009; revised manuscript received 21 September 2009; published 14 December 2009)

We present the formation and structure of vacancy clusters ( $V_n$ ,  $n \leq 48$ ) in crystalline Si based on combined Metropolis Monte Carlo, tight-binding molecular dynamics, and density functional theory calculations. In this size regime, vacancy clusters are predicted to favor fourfold coordination by nullifying dangling bonds created by Si lattice-atom removal. Our results also highlight the identification of a stable high-symmetry  $V_{32}$  configuration that exhibits a complex but ordered tetrahedral core/shell shape. When  $n > 25$ , fourfold-coordinated (FC) clusters commonly show the core/shell figure while smaller FC clusters ( $10 < n < 25$ ) exhibit the trace of the high-symmetry  $V_{12}$  structure that exhibits four identical voidlike structural units surrounding a tetragonal core. In addition, our study reveals that the formation of thermodynamically favored FC clusters can be kinetically facile.

DOI: [10.1103/PhysRevB.80.245209](https://doi.org/10.1103/PhysRevB.80.245209)

PACS number(s): 61.72.jd

## I. INTRODUCTION

Vacancies in crystalline Si (c-Si) have sustained interest because these native defects can greatly influence the mechanical, electrical, and optical properties of the bulk semiconductor. Vacancies are often introduced during manufacturing processes such as ion implantation and crystal growth and expected to predominantly reside in clusters or complexes with other impurities because monovacancies are highly mobile, even at ambient temperatures.<sup>1</sup> Vacancy defects can getter impurities and also recombine with self-interstitials to reduce defect concentrations in active electronic device regions.<sup>2</sup> While the formation of stable voids on the scale of a few nanometers was evidenced by transmission electron microscopy (TEM),<sup>3</sup> direct experimental characterization of small vacancy clusters is challenging because their dimensions often exceed the capabilities of TEM.

A substantial theoretical effort<sup>4-9</sup> has been devoted to the study of vacancy defects in Si. The structure and thermal stability of open-volume defects have been evaluated using extended bond-counting methods, such as “part of hexagonal ring (PHR)” and spherically shaped cluster (SPC) models. However, previous first-principles calculations<sup>6,9</sup> predicted that through structural rearrangements small vacancy clusters ( $V_n$ ,  $3 \leq n \leq 6$ ) tend to favor complete fourfold coordination by nullifying all dangling bonds created by removal of Si lattice atoms. For larger vacancy clusters, fourfold-coordinated (FC) configurations are often too complex to be identified by first-principles calculations alone. To circumvent this obstacle, Lee and Hwang<sup>10</sup> have recently developed an integrated modeling procedure that combines continuous random network model-based Metropolis Monte Carlo (CRN-MMC), tight-binding molecular dynamics (TBMD), and density functional theory (DFT) calculations. Using this combined approach, they demonstrated that FC configurations are thermodynamically more favorable than corresponding PHR or SPC configurations for neutral vacancy clusters up to  $n = 18$ .<sup>11</sup>

Despite this recent progress, some important aspects regarding the structure and formation of larger compact va-

cancy clusters merit elucidation. In particular, few studies have examined the likelihood of high-symmetry configurations for stable FC vacancy clusters, as seen in self-interstitial clusters which exhibit well-ordered extended configurations.<sup>10,12-15</sup> In addition, limited information exists concerning the relative stability between competing FC and PHR/SPC-type structures with cluster size. Finally, little is known regarding the kinetic role in formation of both FC and open-volume (PHR/SPC-type) defects.

In this paper, we present the structure and stability of vacancy clusters up to  $n = 48$  vacancies using a combination of CRN-MMC, TBMD, and DFT calculations. Based on the results, we compare the relative stability between FC and open-volume defects. In addition, our results highlight the identification of an extremely stable FC  $V_{32}$  configuration with high symmetry, which likely influences the growth of larger vacancy structures. We also discuss kinetic feasibility of the formation of thermodynamically favored FC vacancy clusters using TBMD simulation results.

## II. CALCULATION METHODS

The minimum-energy configurations and formation energies of FC vacancy clusters were determined using a combination of CRN-MMC, TBMD, and DFT calculations.<sup>11</sup> For each cluster size, we first generate possible fourfold configurations using CRN-MMC simulations with various initial configurations, followed by TBMD simulations at high temperatures ( $> 1000$  K) to check their thermal stability. Then, we employ DFT calculations to refine the geometries of the stable clusters, and compared their formation energies to determine the lowest-energy structure among them. The details of the integrated computational approach can be found in Refs. 10, 11, and 15.

All atomic structures and energies reported herein were calculated using a plane-wave basis set pseudopotential method within the generalized gradient approximation of Perdew and Wang (GGA-PW91) (Ref. 16) to DFT, as implemented in the Vienna *ab initio* simulation package (VASP).<sup>17</sup> Vanderbilt-type ultrasoft pseudopotentials<sup>18</sup> were used for

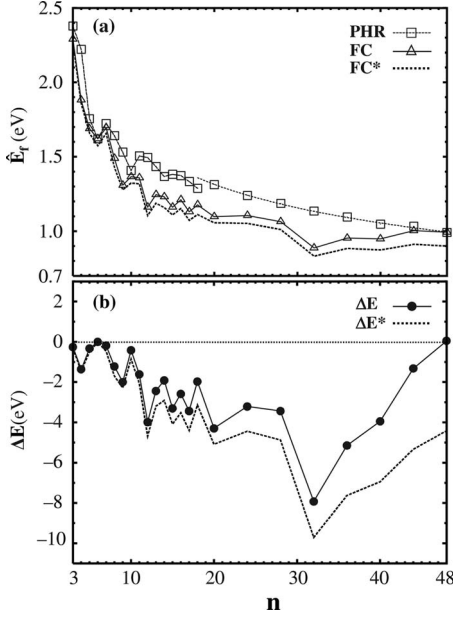


FIG. 1. (a) DFT-predicted formation energies per vacancy ( $\hat{E}_f$ ) of vacancy clusters as a function of cluster size ( $n$ ) for both fourfold-coordinated (indicated as FC) and PHR configurations, together with adjusted values (FC\*) for the FC configurations. For the PHR case of  $n > 18$ , the DFT formation energies per vacancy are well fitted with the power function of  $(-0.82 + 3.68n^{2/3})/n$ , as indicated with a dotted line. (b) Variation in the total-energy difference between the FC and PHR structures from DFT calculations (indicated as  $\Delta E$ ), together with adjusted values ( $\Delta E^*$ ). Refer to the text for the adjustment in the FC-defect formation energies using FF calculations, which is associated with incomplete relaxation of the defect system due to limited supercell size used for DFT calculations.

core-electron interactions. Outer electron wave functions were expanded using a plane-wave basis set with a kinetic-energy cutoff of 160 eV. For Brillouin-zone sampling, we used a  $(2 \times 2 \times 2)$  Monkhorst-Pack  $k$ -point mesh for  $480-n$  and  $576-n$  atom supercells and gamma-point sampling for  $1000-n$  atom supercells. For each defect system, all atoms were fully relaxed using the conjugate gradient method until residual forces on constituent atoms became smaller than  $5 \times 10^{-2}$  eV/Å. The supercell DFT calculations employed a fixed Si lattice constant of 5.46 Å as obtained from volume optimization of defect-free Si. To take into account possible incomplete relaxation of the defect system due to limited supercell size, adjustment of the FC-defect formation energies was also made using force-field (FF) calculations with increasing supercell size. This adjustment appears to be necessary for improved estimation of the formation energies of large FC clusters as discussed later.

### III. RESULTS AND DISCUSSION

Figure 1(a) summarizes the predicted formation energies of PHR and FC vacancy clusters up to  $n=48$ . The formation energy per vacancy [ $\hat{E}_f(n)$ ] is given by  $\hat{E}_f(n) = \{E(N-n) - (1-n/N)E(N)\}/n$ , where  $E(N-n)$  refers to the total energy of an  $N$ -atom supercell with  $n$  vacancies and  $E(N)$  is the total

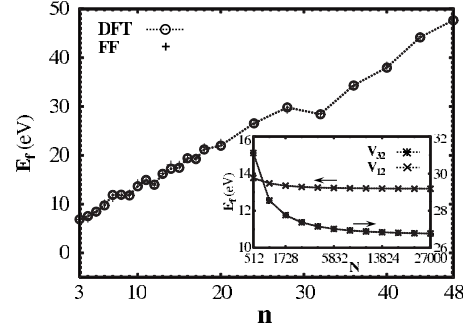


FIG. 2. Comparison of the FC cluster formation energies ( $E_f$ ) between DFT (indicated as DFT) and FF (as detailed in Ref. 11) calculations. The inset shows the  $E_f$  variations in FC  $V_{12}$  and  $V_{32}$  in terms of supercell size;  $N$  indicates the number of Si lattice atoms prior to vacancy defect creation.

energy of an  $N$ -atom bulk Si supercell. Unless noted otherwise, we report formation energies on a per vacancy basis throughout this paper. The total-energy differences between PHR and FC defects are presented in Fig. 1(b), which clearly demonstrates that the FC configurations are energetically more favorable than the PHR configurations for  $3 \leq n \leq 48$ . The energetically favored formation of FC defects indicates that the bond energy gain by fourfold coordination exceeds the strain energy increase via consequent lattice distortions.

For the DFT calculations,  $480-n$ ,  $576-n$ , and  $1000-n$  atom supercells were used for  $V_1-V_{14}$ ,  $V_{15}-V_{18}$ , and  $V_{19}-V_{48}$ , respectively. For the PHR case, the atomic structures of  $n=3-18$  from previous studies<sup>8</sup> were recalculated within DFT-GGA while the other structures of  $n > 18$  were constructed by optimizing initial structures which were prepared to have minimum dangling bonds. For the formation-energy calculation, highly strained FC structures commonly require larger supercells than PHR structures. To avoid large and computationally expensive supercells, we adjusted the formation energies [ $E_f(n) = n\hat{E}_f(n)$ ] for the DFT calculation with  $E_f(n)$  from the FF calculations (as described in Ref. 11),  $E_f(n) = E_f^{\text{FF}}(n, N_L) + \{E_f^{\text{DFT}}(n, N_S) - E_f^{\text{FF}}(n, N_S)\}$ , where superscripts FF and DFT indicate values calculated from their respective methods, and  $N_L$  and  $N_S$  represent large (27 000 atoms which is  $15 \times 15 \times 15$  times larger than a eight-atom cubic cell) and small ( $\leq 1000$  atoms employed for DFT calculations) supercells, respectively, both without defects. The discrepancies between the DFT (indicated as FC) and adjusted (FC\*) values in Fig. 1(a) indicate the importance of the adjustment.

We also carefully checked the validity of the adjustment approach. As illustrated in Fig. 2, the DFT [ $E_f^{\text{DFT}}(n, N_S)$ ] and FF [ $E_f^{\text{FF}}(n, N_S)$ ] values for the FC  $V_n$  defects in these small ( $N_S \leq 1000$  atoms) supercells are almost identical, implying that the FF method is adequate to estimate the formation energies of FC defects. This is not surprising considering the well-relaxed FC structures show no significant departure from crystalline Si, and thus their energetics can be described reasonably well by Keating-type potentials.<sup>10,11,15</sup> The inset of Fig. 2 exhibits the variations in  $E_f^{\text{FF}}(n, N_L)$  for FC  $V_{12}$  and FC  $V_{32}$  with increasing  $N_L$ . The result demonstrates that the  $E_f^{\text{FF}}(n, N_L)$  values nearly saturate when  $N_L \approx 27$  000 while the

smaller case ( $V_{12}$ ) converges much faster, confirming the soundness of our choice of  $N_L=27\,000$  atoms for the adjustment of the formation energies of FC defects.

One important feature from our calculations is that the FC-defect formation energy appears to saturate for  $n>30$  (although some variation with  $n$  still occurs) while the PHR-defect formation energy monotonically decreases. As a result, the total-energy difference between the FC and PHR states peaks at  $n=32$ , then gradually decays; for  $n\gg 50$ , the PHR state is expected to be energetically more favorable than the FC state. This further supports our previous conclusion<sup>11</sup> that the  $E_f(n)$  of voidlike defects (such as PHR defects) is largely governed by the void-surface energy which is proportional to void-surface area ( $\sim n^{2/3}$ ) whereas the  $E_f(n)$  of FC defects is determined by the number of strained Si atoms which is proportional to cluster size ( $\sim n$ ). Therefore, we expect the formation energy per vacancy in the PHR case to monotonically decrease ( $\sim n^{2/3}/n=n^{-1/3}$ ) while the FC case instead saturates and becomes size independent ( $\sim n/n=1$ ).

Another, perhaps most important, observation is the existence of an extremely stable FC  $V_{32}$  configuration with a  $\hat{E}_f(n)$  of only 0.89 and 0.83 eV before and after adjustment, respectively. To better understand its remarkable stability we analyze the atomic configuration of FC  $V_{32}$  in Fig. 3. The FC  $V_{32}$  structure contains an “adamantine cage” (AC) core surrounded by a distorted shell and exhibits tetrahedral geometry with four triangular (111) facets and four corners. The covalent network inside the shell region is distorted and under tension but also shows a characteristic pattern of  $n$ -membered rings consistent with the overall cluster symmetry. The six edges along the tetrahedron boundary are each defined by two essentially parallel and approximately linear chains of five Si atoms. Figure 3 illustrates the subtle differences among the six cluster edges while Fig. 3(b) conveys the overall symmetry of FC  $V_{32}$  and indicates that the six edges of FC  $V_{32}$  are not all identical. We define four edges as parallel and two edges as antiparallel. The atomic-level detail of Figs. 3(a) and 3(c) contrast how the two edges are different. In the antiparallel edges, the bonded atoms among the five constituents of each chain are staggered. In the parallel edges, the bonded atoms among the five members of each chain are arranged side by side. Note that the alignment of unbonded atoms between the two parallel chains is responsible for an eight-atom ring on each of these edges. If the linear arrangement of one of the five-membered chains of the antiparallel edge is reversed, a parallel edge configuration results. Despite the variations in edge structure, the four (111) faces and four corners are identical to each other, respectively. Therefore, the approximately regular tetrahedron, which has one  $C_2$  axis and two  $S_4$  rotation-reflection axes, is characterized by  $S_{24}$  symmetry.

It is worth emphasizing that each of the four corner regions of the FC  $V_{32}$  tetrahedron resembles the  $C_2$  symmetry FC  $V_{12}$  structure that is comprised of four identical voidlike structural units surrounding a tetragonal core.<sup>11</sup> Figure 3(d) shows that the band gap in the presence of  $V_{32}$  is free of additional defect states and is essentially the same as the c-Si gap. The enhanced stability of FC  $V_{32}$  is likely attributed to its unique crystalline core and symmetric, yet distorted,

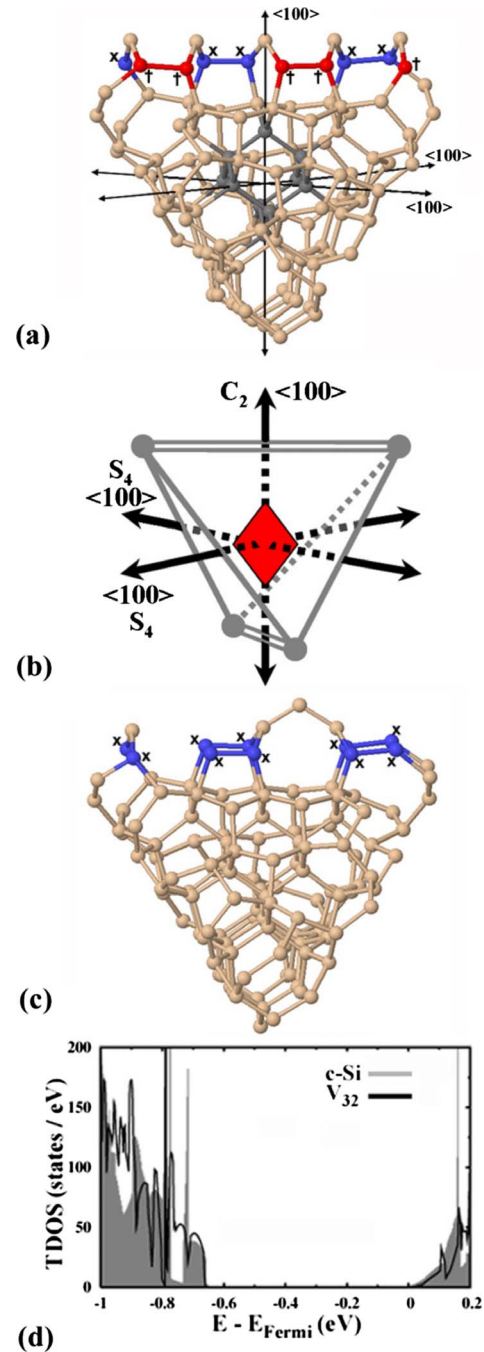


FIG. 3. (Color online) (a) Core and strained nearest neighbors of FC  $V_{32}$  shown isolated from bulk Si lattice. In (a), we annotate the antiparallel edge type, where member atoms of each chain are distinguished by either “x” or “+” labels (blue or red spheres, respectively). The ten atoms comprising the AC in the center of the structure are identified as dark gray spheres. (b) Illustration of a simplified geometric diagram of FC  $V_{32}$  that highlights the  $S_{24}$  group symmetry, AC core, and the two antiparallel (double line) and four parallel (single line) cluster edges. Axis labels denote cluster orientation with respect to the Si lattice. (c) Reorientation of FC  $V_{32}$  to emphasize the parallel edge, where atoms comprising these chains are annotated with x labels (blue spheres). (d) Total density of states comparison of bulk Si to  $V_{32}$  near the band gap using 1000-atom basis supercells with the conduction-band edges set as references.

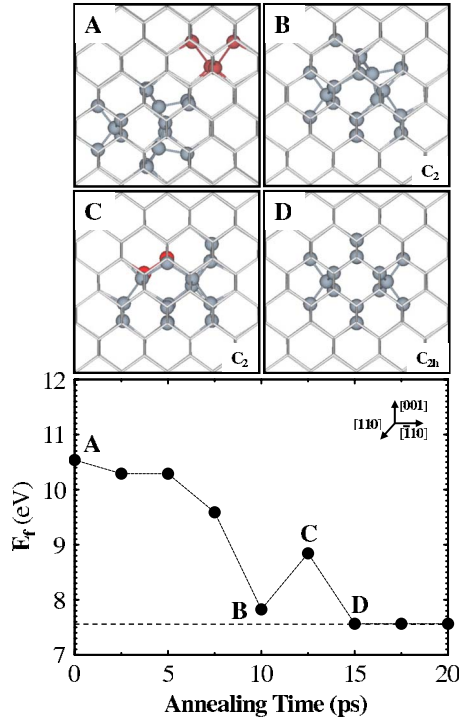


FIG. 4. (Color online) Monovacancy-induced structural rearrangement, together with variation in the formation energy ( $E_f = n\hat{E}_f$ ) as a function of annealing time for  $V_3+V \rightarrow V_4$  during TBMD simulations at 1400 K. All atomic configurations from the TBMD simulation were optimized within DFT-GGA calculations using gamma-point BZ sampling for  $512-n$  atom supercells and illustrated in the top and middle panels. Grey wire frame represents bulk Si lattice and dark grey spheres represent highly strained FC atoms. Si dangling defects are also depicted by red (black) spheres.

covalent-bond topology in the shell region. We also find that when  $n > 25$  the stable FC clusters identified here commonly show the core/shell-like arrangement (with an AC core) while smaller FC clusters ( $10 < n < 25$ ) exhibit the trace of ordered  $V_{12}$ .<sup>11</sup> The atomic configurations of other FC clusters will be presented elsewhere.

Next, we examine if the formation of FC vacancy defects can also be kinetically favored over their PHR counterparts. Vacancy defects may grow by capturing mobile single vacancies (and possibly also divacancies<sup>19,20</sup>) from the crystalline matrix. In addition, vacancy clusters may also be formed by recrystallization of low-density amorphous regions that are deficient in Si atoms compared to the perfect crystal. To investigate vacancy cluster growth, we performed TBMD simulations at 1400 K for several systems of small clusters ( $V_n$ ,  $n=2-4, 11$ ), each of which had an additional monovacancy in close proximity.

Figure 4 illustrates  $V_3+V \rightarrow V_4$ , where the initial FC structure of  $V_3$  is quickly perturbed upon capturing a monovacancy and yields multiple coordination defects (CDs), i.e., dangling and floating bonds. The intermediate structure undergoes successive rearrangements that render a stable PHR structure around 12.5 ps, which subsequently relaxes to the lowest-energy FC structure with  $C_{2h}$  symmetry within 15 ps. Similarly, as shown in Fig. 5, the  $V_{11}+V \rightarrow V_{12}$  case leads to the lowest-energy FC  $V_{12}$  structure with  $C_2$  symmetry within

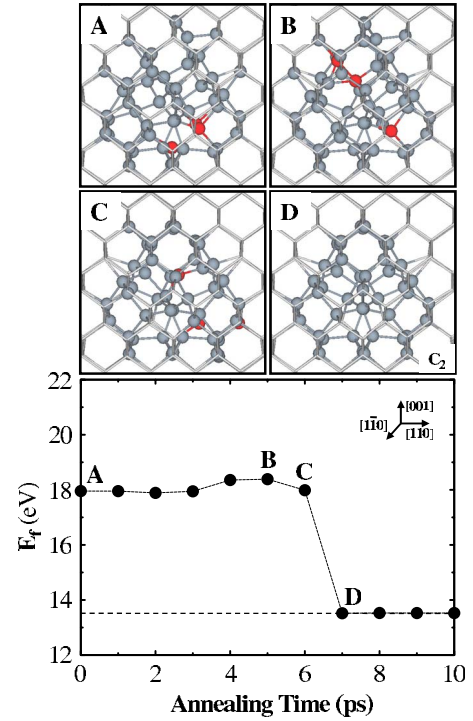


FIG. 5. (Color online) Monovacancy-induced structural rearrangement, together with variation in the formation energy ( $E_f = n\hat{E}_f$ ) as a function of annealing time for  $V_{11}+V \rightarrow V_{12}$  during TBMD simulations at 1400 K. All atomic configurations from the TBMD simulation were optimized within DFT-GGA calculations using gamma-point BZ sampling for  $512-n$  atom supercells and illustrated in the top and middle panels. Grey wire frame represents bulk Si lattice and dark grey spheres represent highly strained FC atoms. Si dangling defects are also depicted by red (black) spheres.

7 ps. During the agglomeration, multiple CDs arise and diffuse around the cluster, which in turn enhances structural rearrangement while the majority of Si atoms in the cluster region remain fourfold coordinated.

For the  $V_2+V \rightarrow V_3$  and  $V_4+V \rightarrow V_5$  cases, the overall agglomeration mechanisms are similar to the  $V_3+V \rightarrow V_4$  and  $V_{11}+V \rightarrow V_{12}$  cases. However, after 20 ps of the TBMD simulations, the  $V_3$  and  $V_5$  aggregates did not complete fourfold coordination. We continued the TBMD simulations for additional 20 ps (=40 ps total). As shown in Fig. 6, the  $V_5$  ended up with the lowest-energy FC configuration around 35 ps but the  $V_3$  was not fully fourfold coordinated after 40ps of the TBMD simulation. The relatively slow reconfigurations of the  $V_3$  and  $V_5$  aggregates to their lowest-energy FC configurations can be related to the small energy differences of 0.26 and 0.33 eV, respectively, between the FC and PHR states; in contrast, the fourfold coordination of  $V_4$  and  $V_{12}$  yields significant energy gains of 1.36 and 3.99 eV (before adjustment) over their PHR counterparts. In particular, the  $V_3$  FC structure is highly strained and thus can be easily ruptured by generating CDs during the high-temperature annealing at 1400 K, retarding the fourfold coordination that leads to its lowest-energy state.

Using TBMD simulations at 1400 K, we proceeded to evaluate the structural evolution of amorphous pockets with atomic Si deficiencies. We employed CRN-MMC simula-

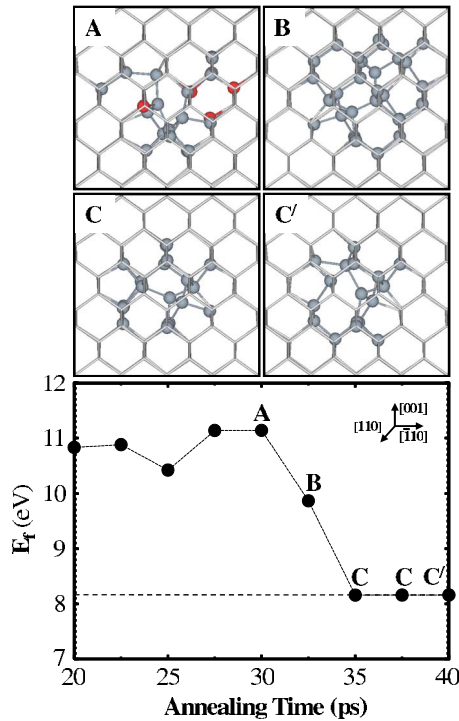


FIG. 6. (Color online) Monovacancy-induced structural rearrangement, together with variation in the formation energy ( $E_f = n\hat{E}_f$ ) as a function of annealing time for  $V_4 + V \rightarrow V_5$  during TBMD simulations at 1400 K. All atomic configurations from the TBMD simulation were optimized within DFT-GGA calculations using gamma-point BZ sampling for  $512-n$  atom supercells and illustrated in the top and middle panels. Grey wire frame represents bulk Si lattice and dark grey spheres represent highly strained FC atoms. Si dangling defects are also depicted by red (black) spheres.

tions to prepare initial amorphous pocket structures embedded in c-Si supercells. For each model amorphous system in our statistical sample, 12 atoms were deficient in the amorphous region relative to c-Si but all constituent Si atoms remained fourfold coordinated. Consequently, complete recrystallization will leave 12 vacancies. Among four independent model systems evaluated, one case yielded the lowest-energy FC  $V_{12}$  with  $C_2$  symmetry within 20 ps as shown in Fig. 7 (dark circle). Upon annealing, the amorphous pocket is relaxed via bond rearrangements assisted by coordination defects and subsequently leads to its recrystallization from the interface between the amorphous and crystalline regions. After 17 ps, the FC  $V_{12}$  configuration is formed and remains virtually unchanged throughout the remainder of the 60 ps simulation. For another two cases, the amorphous pockets gradually transformed into the lowest-energy FC  $V_{12}$  state but were not completed within the 60 ps simulation duration.

As shown in the inset of Fig. 7, our TBMD simulations also show the possibility that an amorphous pocket would evolve into a PHR defect. We noticed that the PHR-defect formation can take place if the rate of CD creation by breaking highly strained Si-Si bonds is higher than that of CD annealing through bond network rearrangements (i.e., when several Si-Si bonds are ruptured for a short period of time within which annealing of the created CDs seldom occurs). The nearly simultaneous rupture of multiple Si-Si bonds

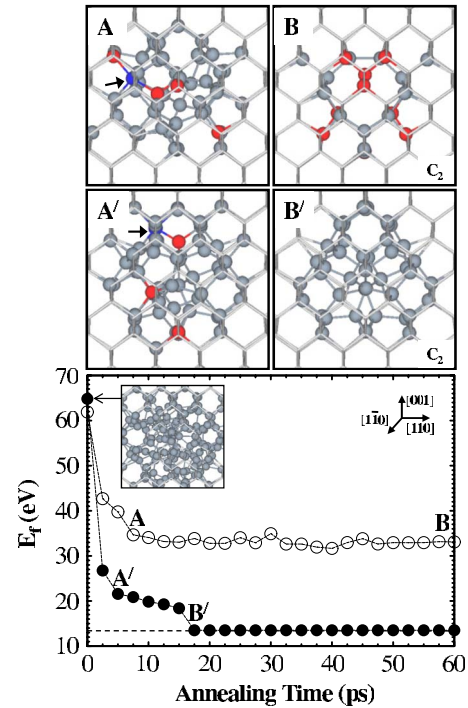


FIG. 7. (Color online) Structural evolution of amorphous pockets with deficit of 12 atoms during TBMD simulations at 1400 K together with variation in the formation energy ( $E_f = n\hat{E}_f$ ) as a function of annealing time. All atomic configurations from the TBMD simulation were optimized within DFT-GGA calculations using gamma-point BZ sampling for  $512-n$  atom supercells. Filled circles illustrate the formation of the lowest-energy FC  $V_{12}$  with  $C_2$  symmetry, together with their atomic configurations as indicated. Open circles illustrate the formation of a PHR  $V_{12}$  structure, together with their atomic configurations as indicated; however, the PHR-defect formation would be rather unlikely in a typical annealing process, as discussed in the text. Grey wire frame represents bulk Si lattice and dark grey spheres represent highly strained FC atoms. Si dangling and floating bonds are depicted by red (black) and blue (black, indicated by the arrow) spheres, respectively.

could be possible only when the amorphous network is significantly strained and also under immediate high-temperature treatment, like the condition employed in the TBMD simulation above. However, a typical annealing process involves a ramp-up period during which we expect a highly strained network would be gradually relaxed without the nearly simultaneous break of multiple Si-Si bonds. This leads us to speculate that the formation of open-volume PHR type defects would be rather unlikely during recrystallization of an amorphous region, especially when the amorphous pocket is large enough so that it can be rearranged without inducing significant local strains. While the creation of PHR defects cannot be excluded during processing, for completeness we also performed TBMD at 1400 K starting with the PHR  $V_{12}$  configuration but there was no indication for PHR  $\rightarrow$  FC conversion although dangling bonds underwent diffusion along the cluster surface. This suggests that there exists a sizable barrier for the PHR  $\rightarrow$  FC transformation for sufficiently large vacancy defects, which is not surprising considering the significant lattice distortions required for

linking the under-coordinated Si atoms to be fourfold coordinated. The results may also indicate that PHR defects could coexist with FC defects while the latter are likely to be prevailing.

Although further studies might be necessary to verify the kinetic role in the structural evolution of various  $V_n$  clusters, our work suggests the possible formation of thermodynamically favored FC vacancy clusters for  $n < 48$  with no significant kinetic limitations. This suggests that a large fraction of small vacancy defects can exist in the FC state in c-Si. However, it appears to be impractical to explicitly characterize FC vacancy clusters with currently available spectroscopic techniques because of their optically inactive nature (given no energy states within the Si band gap [see Fig. 3(d)]). Nonetheless, the presence of FC defects could be expected to alter the properties and behavior of Si materials such as thermal conductivity, elastic modulus, and impurity gettering. Further studies are therefore warranted to better understand the formation and nature of FC vacancy defects together with open-volume PHR-type defects, particularly their effects on the thermal/electrical transport, mechanical, and gettering properties of Si-based nanomaterials for future thermoelectric and electronic applications.

#### IV. SUMMARY

We have examined the formation, structure, and stability of vacancy clusters up to  $n=48$  vacancies using a combina-

tion of CRN-MMC, TBMD, and DFT calculations. In this size regime our calculations demonstrate that FC configurations are energetically more favorable than PHR structures; however, with increasing cluster size (up to a few nanometers in diameter) less strained open-volume PHR-type defects will be ultimately favored as the energy penalty from strained atoms in FC clusters overwhelms energy gains from minimized dangling-bond density. Our results highlight the identification of an extremely stable FC  $V_{32}$  configuration that exhibits a complex but ordered tetrahedral shape containing an adamantane cage core surrounded by a distorted shell. When  $n > 25$  stable FC clusters commonly show the core/shell feature while smaller FC clusters ( $10 < n < 25$ ) exhibit the trace of ordered  $V_{12}$  that is comprised of four identical voidlike structural units surrounding a tetragonal core.<sup>11</sup> Our TBMD simulations also suggest that the formation of thermodynamically favored FC vacancy clusters could be kinetically facile. Our findings emphasize the importance of better understanding the nature of stable FC vacancy defects to effectively estimate and manipulate the properties and behavior of Si-based materials.

#### ACKNOWLEDGMENTS

We acknowledge National Science Foundation (Contract No. CAREER-CTS-0449373) and Robert A. Welch Foundation (Contract No. F-1535) for their financial support. We would also like to thank the Texas Advanced Computing Center for use of their computing resources.

---

\*Author to whom correspondence should be addressed; gshwang@che.utexas.edu

<sup>1</sup>G. D. Watkins, J. W. Corbett, and R. M. Walker, *J. Appl. Phys.* **30**, 1198 (1959).

<sup>2</sup>V. C. Venezia, D. J. Eaglesham, T. E. Haynes, A. Agarwal, D. C. Jacobson, H.-J. Gossmann, and F. H. Baumann, *Appl. Phys. Lett.* **73**, 2980 (1998).

<sup>3</sup>J. S. Williams, M. J. Conway, B. C. Williams, and J. Wong-Leung, *Appl. Phys. Lett.* **78**, 2867 (2001).

<sup>4</sup>D. J. Chadi and K. J. Chang, *Phys. Rev. B* **38**, 1523 (1988).

<sup>5</sup>G. H. Gilmer, T. Diaz de la Rubia, D. M. Stock, and M. Jaraiz, *Nucl. Instrum. Methods Phys. Res. B* **102**, 247 (1995).

<sup>6</sup>J. L. Hastings, S. K. Estreicher, and P. A. Fedders, *Phys. Rev. B* **56**, 10215 (1997).

<sup>7</sup>A. La Magna, S. Coffa, and L. Colombo, *Phys. Rev. Lett.* **82**, 1720 (1999).

<sup>8</sup>T. E. M. Staab, A. Sieck, M. Haugk, M. J. Puska, Th. Frauenheim, and H. S. Leipner, *Phys. Rev. B* **65**, 115210 (2002).

<sup>9</sup>D. V. Makhov and L. J. Lewis, *Phys. Rev. Lett.* **92**, 255504 (2004).

<sup>10</sup>S. Lee and G. S. Hwang, *Phys. Rev. B* **77**, 085210 (2008); **78**, 045204 (2008); S. Lee, R. J. Bondi, and G. S. Hwang, *Mol. Simul.* **35**, 867 (2009).

<sup>11</sup>S. Lee and G. S. Hwang, *Phys. Rev. B* **78**, 125310 (2008).

<sup>12</sup>M. Kohyama and S. Takeda, *Phys. Rev. B* **46**, 12305 (1992).

<sup>13</sup>J. Kim, J. W. Wilkins, F. S. Khan, and A. Canning, *Phys. Rev. B* **55**, 16186 (1997).

<sup>14</sup>J. Kim, F. Kirchhoff, J. W. Wilkins, and F. S. Khan, *Phys. Rev. Lett.* **84**, 503 (2000).

<sup>15</sup>R. J. Bondi, S. Lee, and G. S. Hwang, *Phys. Rev. B* **79**, 104106 (2009); *Appl. Phys. Lett.* **94**, 264101 (2009); *Phys. Rev. B* **80**, 125202 (2009).

<sup>16</sup>J. P. Perdew and Y. Wang, *Phys. Rev. B* **45**, 13244 (1992).

<sup>17</sup>G. Kresse and J. Furthmüller, *VASP the Guide* (Vienna University of Technology, Vienna, 2001).

<sup>18</sup>D. Vanderbilt, *Phys. Rev. B* **41**, 7892 (1990).

<sup>19</sup>G. S. Hwang and W. A. Goddard III, *Phys. Rev. B* **65**, 233205 (2002).

<sup>20</sup>D. A. Abdulmalik and P. G. Coleman, *Phys. Rev. Lett.* **100**, 095503 (2008).